Appl. Phys. A 66, 59–67 (1998)

Applied Physics A
Materials
Science & Processing

Prevention of micropipes and voids at β-SiC/Si(100) interfaces

R. Scholz[1], U. Gösele[1], F. Wischmeyer[2], E. Niemann[2]

[1] Max-Planck-Institut für Mikrostrukturphysik, D-06120 Halle/Saale, Germany
(Fax: +49-345/5582-566, E-mail: roscholz@mpi-halle.mpg.de)
[2] Daimler-Benz Forschungsinstitut, D-60528 Frankfurt/Main, Germany
(Fax: +49-69/6679-322, E-mail: ZF2M053@dbag.fra.daimlerbenz.com)

Received: 23 April 1997/Accepted: 30 July 1997

Abstract. Chemical vapor deposition (CVD) carbonization experiments were carried out on (100) silicon substrates. Scanning and transmission electron microscopy (SEM and TEM) were used to detect and characterize the interface defects. Conditions for preventing the formation of micropipes and voids at the SiC/Si interfaces were found.

PACS: 61.16; 68.35; 68.55

Single crystalline silicon carbide is an attractive semiconductor for high temperature and power electronics applications [1, 2] as well as a substrate for the epitaxial growth of GaN-based layers for light emitting diodes and lasers [3]. Presently, single crystalline SiC wafers (in the hexagonal form 6H) are available only in diameters below about 3 cm and for prices in the order of \$1000/wafer. Consequently, there are development efforts underway to increase the wafer diameter or, in order to decrease the costs of SiC layers used for further heteroepitaxial growth, to transfer thin ($< 1\,\mu$m) single crystalline 6H-SiC layers onto an appropriate comparatively inexpensive substrate such as silicon, glass or polycrystalline SiC. This transfer process by the smart-cut approach involves hydrogen implantation and direct wafer bonding and allows the starting 6H−SiC wafer to be reusable for further layer transfers [4, 5]. Alternatively, in order to be able to produce single crystalline SiC layers over large wafer areas typical for silicon technology, epitaxial growth of SiC (in the cubic form of β-SiC) on single-crystalline silicon has been investigated for many years. Because of the large lattice mismatch, this approach is plagued by a relatively high density of planar lattice defects. The best crystal quality is generally obtained if the initial SiC layer is formed by carbonization of the silicon [6], a process which, however, frequently causes the formation of pyramidal voids [7–14] and micropipes [15, 16] at the SiC/Si interface by out-diffusion processes of silicon atoms which then react with the carbon (supplied in the form of a hydrocarbon gas) to form SiC.

The present paper reports on a variety of carbonization experiments which allow one to determine under which conditions extended out-diffusion defects form and under which conditions they may be prevented. We will first describe the previous state of understanding of micropipe and void formation before turning to the actually performed new carbonization experiments and the associated electron microscopical analysis.

Detection, characterization, and a proposed model of micropipe defects forming at β-SiC/Si(100) interfaces have already been described [15, 16]. These micropipes form in CVD carbonization experiments as a second type of Si-outdiffusion defects within the substrate surface besides the more common voids which occur as inverted pyramids [7–14]. Such pyramidal voids are also known to develop under SiC layers grown on silicon substrates by applying other deposition methods (for references see e.g. [13, 16]). While voids remain empty during silicon out-diffusion and become bridged by the growing SiC layer, micropipes develop by Si out-diffusion and simultaneous ingrowth of SiC. Micropipe densities are orders of magnitude higher than void densities. Micropipe formation was attributed to the unusual pretreatment and carbonization regime applied to the silicon substrates in our previous experiments [16]. In these experiments, the substrates were annealed on C-containing susceptors under hydrogen flow for 1 h at 1300 °C which causes a high density of SiC contamination nuclei on the surfaces before carbonization. These preexisting nuclei favoured the micropipe formation. Initial forms of micropipes were detected which had their SiC-coated crater-like origins in gaps between SiC islands developing from these nuclei. Pyramidal voids of common density were observed amid the micropipe defects of high density.

The first TEM results from specimens of our new experiments aimed at the prevention of voids and micropipes, based on a drastic change of the pretreatment, indicated that micropipes can also develop by carbonization initiated during a temperature ramp-up procedure with no SiC nuclei occuring after the pretreatment [17]. The present paper describes details of the results of these carbonization experiments, in

particular showing the way in which voids and micropipes can be prevented.

1 Experiments

As a first step in the new experiments (as compared with our previous carbonization experiments [15, 16]), C_3H_8 was used instead of C_2H_4 as the reactive gas. Then, a short-time carbonization experiment was carried out with C_3H_8 gas, with the initial pretreatment and the carbonization regime kept unchanged (experimental regime 1), to check whether micropipes also develop with the new reaction gas. The experimental conditions were identical to those of the 10 s carbonization experiment described in [16] (1220 °C substrate temperature, 80 mbar total pressure, 3.5 slm H_2 flow). 14 sccm C_3H_8 were added for only 1 s to the H_2 flow as the substrate was at high temperature. As before within the CVD reactor, in all the experiments an SiC-coated graphite susceptor was used for silicon (100) substrates of 1 inch in diameter (2° to 4° off-axis).

To keep the initial conditions constant throughout the new series of experiments, after each carbonization the unloaded susceptor was carefully cleaned. The pretreatment of the substrates was drastically changed compared with that in the first experiments [16]; it consisted of an anneal on the cleaned susceptor in a hydrogen flow of 3.5 slm at 1000 °C for only 5 min, applying a total pressure of 80 mbar. SEM and cross-section TEM checks of pretreated substrates showed perfect surfaces without any SiC crystallites or etch pits.

Based on the experimental data which allowed us to avoid pyramidal voids during carbonization [18], after cooling the substrates to 500 °C, the C_3H_8 reaction gas was added to the continuous H_2 flow, followed by a slow temperature ramp-up procedure of 200 °C/min until the respective carbonization temperature was reached. Further parameters of the new series of experiments considered here (regime 2) are summarized in Table 1. Total pressures of 50, 100 and 150 mbar, respectively, were chosen instead of the atmospheric pressure used in [18] and in many other experiments. The hydrocarbon gas fractions of 0.33, 0.66 and 1 sccm added to the unchanged hydrogen flow of 3.5 slm, are much lower than in former carbonization experiments. Therefore, our new experiments probably cover a range of parameter variations which had not been selected before in combination with such a slow temperature ramp. The substrates were only carbonized with no layer growth following. The carbonized silicon substrates were investigated by SEM in a JSM-6300F microscope at relatively low primary voltages. Cross-section and planar specimens were studied by TEM in 100 kV JEM-100C, 400 kV JEM-4000EX and 200 kV CM20T microscopes.

2 Experimental results

2.1 Carbonization with C_3H_8 instead of C_2H_4 under experimental regime 1

Carbonization with C_3H_8 for 1 s at 1220 °C confirmed the formation of micropipes and at the same time the existence of pyramidal voids of extremely large size; these had never been observed in our previous experiments with C_2H_4 gas. However, such void sizes are quite often quoted in the literature (base lengths in the order of 1 μm, see, e.g., [7, 8, 11, 13]). The SEM image of Fig. 1a shows a number of voids, whereas Fig. 1b (at larger magnification) shows just one void with an irregular cover but otherwise grainy structure of the surface surrounding. Figure 1c (still larger magnification) reveals gaps between these grains similar to those described in [16, 17] for the 10 s carbonization with C_2H_4 gas. The cover over the large voids consists of an incomplete, highly porous network of a SiC layer, which seems partly to hang over the pits in the silicon surface. Experiments of growth of SiC on Si [19] revealed similar features. Figure 1d (the same magnification as Fig. 1c) is a plan-view TEM image of a thin sandwich sample of SiC on Si, showing, at relatively large defocus, the contrast of the gaps in the SiC surface with a density comparable to that in the SEM image of Fig. 1c.

A cross-section TEM (Fig. 2) of this sample revealed the following differences in details from those of the 10 s carbonization using C_2H_4 [16]. As expected, the grainy surface structure is due to an SiC coverage consisting of coalesced grains of different heights (Fig. 2a). The long surface facets of the SiC grains are (100) faces. They are inclined to the

Table 1. Parameters for the new series of CVD carbonization experiments, with results as to interface defects observed and the SiC layer thickness measured. The heating rate was always 200 °C/min

Experiment, wafer, run #	Total pressure (mbar)	C_3H_8 in 3.5 slm H_2 (sccm)	Substrate temperature (°C)	Carbonization time (s)	Voids (cm^{-2})	Micropipes (cm^{-2})	SiC Layer thickness (nm)
594	50	0.33	1340	60	yes	4×10^9	18 (25)
598	150	0.33	1340	60	10^6	no	4 (6)
600	100	0.33	1340	60	yes	8×10^9	6 (12)
602	100	0.33	1340	10	yes	8×10^9	6 (8)
604	50	0.33	1290	60	yes	4×10^9	12 (18)
606	100	0.33	1290	60	yes	8×10^9	5 (6)
608	150	0.33	1290	60	10^6	no	3 (5)
612	50	0.66	1290	60	yes	1.2×10^{10}	6.5 (8)
614	100	0.66	1290	60	no	no	2 – 3
616	150	0.66	1290	60	no	no	2.5 – 3
620	50	1	1290	60	no	no	1.2 – 2
622	100	1	1290	60	no	no	2
626	150	1	1290	60	no	no	2.3

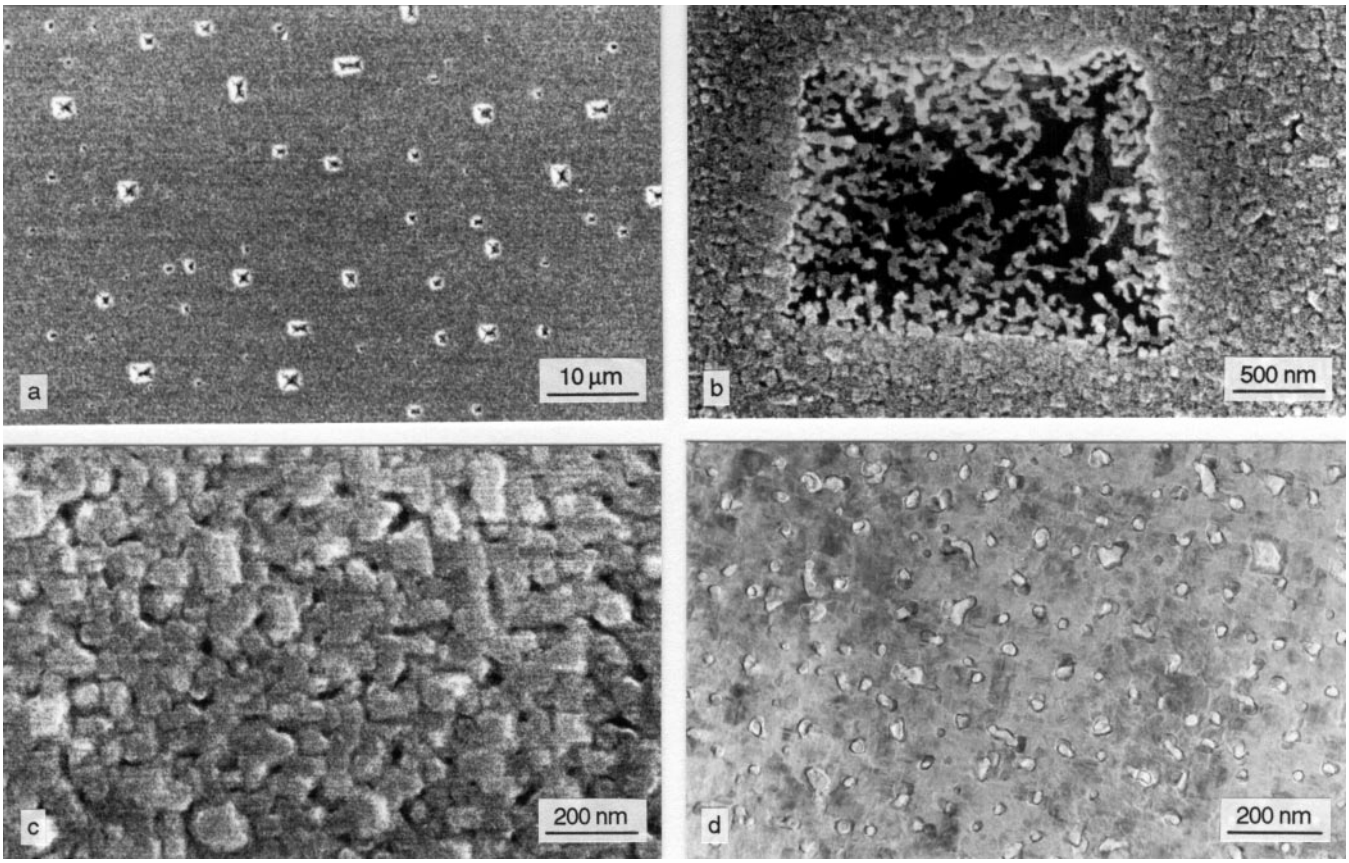

Fig. 1a–d. SEM images at different magnification (**a**–**c**) and a plan-view TEM image (**d**) of a carbonization experiment of 1 s, using C_3H_8 reaction gas under the old experimental regime 1

SiC/Si interface corresponding to the off-axis orientation of the original substrate surface. In the gaps between the grains, micropipes begin to form, which after 1 s of carbonization are larger and of different shape from those obtained after 10 s of carbonization with C_2H_4. The tips of the pipes within the substrate are distinctly faceted along {111} faces, but are not as elongated as before (see Figs. 11 and 12 in [16]). Furthermore, the mean thickness of the SiC layer grown in C_3H_8 flow for 1 s is obviously larger than before, owing to the larger amount of silicon consumed by the larger pipes. Steckl and Li [20] pointed out that carbonization with C_3H_8 gas instead of C_2H_4 created much thicker SiC layers under their specific experimental conditions which, however, differ from ours.

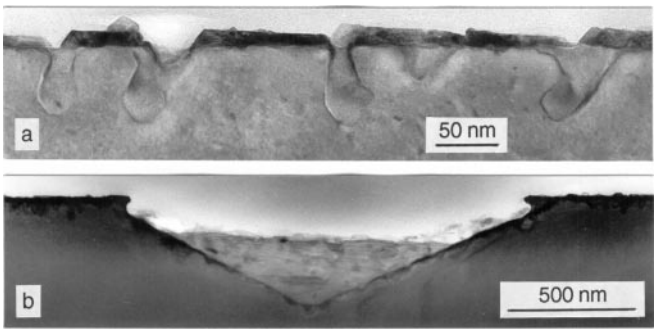

Fig. 2a,b. TEM cross-section results of the carbonization experiment of 1 s, using C_3H_8. Initial shapes of micropipes below gaps within the SiC cover layer (**a**), and a large void bounded by {311}-type faces of the substrate (**b**)

Some individual large voids revealed by SEM are also detected in TEM cross-sections (cf. Fig. 2b). The large pyramidal voids are not bounded by {111}-type faces within the substrate, as carbonization-induced voids usually are, but by faces of type {311}. The fragile SiC layer covering these voids (Fig. 1b) is not maintained in the cross-sections due to the preparation procedure. However, some remnants are enclosed in the glue within the pits. Close inspection of the TEM cross-sections and plan-view observations mentioned above reveal that the {311} borders of these voids are also covered with a grainy SiC layer of a thickness similar to that of the (100) surface. Micropipe formation is weakly indicated at the {311} walls (cf. Fig. 2b). The origin of these large voids will not be considered further in this paper. SEM images (cf. Fig. 1a) reveal a void density of about 10^6 cm^{-2}, and plan-view TEM images (cf. Fig. 1d) show a pipe density of about 10^{10} cm^{-2}.

2.2 Carbonization under experimental regime 2

2.2.1 SEM results of carbonized silicon surfaces with interface defects. SEM investigations of surfaces carbonized under the conditions given in Table 1 revealed defect structures or contrasts only for experimental runs #594–612. All the other experiments (#614–626) did not indicate any contrast in the SEM that would point to surface or interface defects. The main features revealed by SEM are summarized in Figs. 3a–d, reflecting experiments #604, 606, 608 and 612. The carbonization temperature was always 1290 °C,

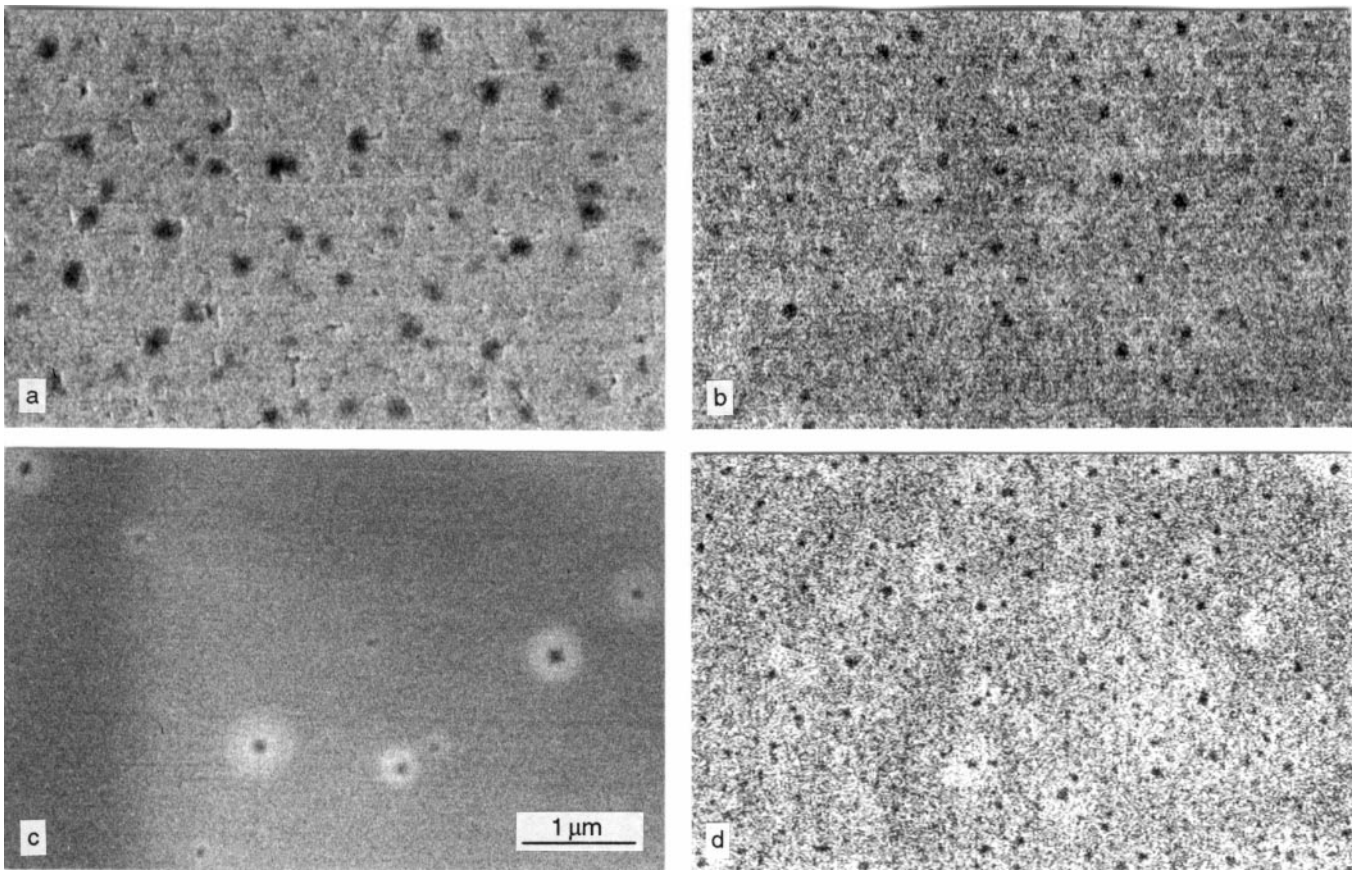

Fig. 3a–d. SEM results obtained from carbonization experiments under the new regime 2. The different defect structures of experiments #604 (**a**), 606 (**b**), 608 (**c**) and 612 (**d**). Increasing the total pressure of 50, 100, and 150 mbar in (**a**) to (**c**), and doubling the C_3H_8 flow at 50 mbar in (**d**) (see Table 1)

with the total pressure varying. In one case (#612), a higher hydrocarbon gas flow was used at the lowest pressure applied (50 mbar).

Based on similar published results of this kind [7, 9, 11–13, 21], we attribute the dark features in the images to voids under the SiC cover of the substrate. The void size varies between about 250 nm in base length (see Fig. 3a) and far below 100 nm (see Figs. 3b,d). Only Fig. 3a shows some additional gaps in the top layer comparable to the gaps above the micropipes observed in our previous short-time carbonization experiments under regime 1. As to sample #606 (Fig. 3b), similar gaps of smaller size and higher density were observed by SEM at higher magnification. Unlike previous results, here the surfaces do not show a distinct grain structure as, e.g., in Fig. 1c, suggesting a much lower roughness of the SiC surfaces. The void densities measured in the SEM images of samples #604 and 606 are in the order of about 2 to $4 \times 10^8\,\mathrm{cm}^{-2}$, and of sample #612, about $10^9\,\mathrm{cm}^{-2}$. The overall void density of wafer #608 (Fig. 3c) is about $10^6\,\mathrm{cm}^{-2}$. Similar results were attained for the other carbonization conditions within the range #594–602. It is worth noting that there was no change in the size and density of most of the small dark contrast features when the carbonization time was changed from 10 s to 60 s (#602 and 600). Therefore, most of these defects are already present after 10 s of carbonization, and do not grow any further subsequently.

SEM observations of the samples prepared by our new carbonization experiments indicate that, depending on the specific carbonization conditions, voids and possibly micropipes may be formed or prevented.

2.2.2 TEM results of carbonized silicon surfaces with interface defects. Our TEM investigations confirmed the presence of micropipes in addition to voids in several samples as was indicated by the SEM observations. Figures 4a,b show two cross-sectional images from experiments #594 and 606, at

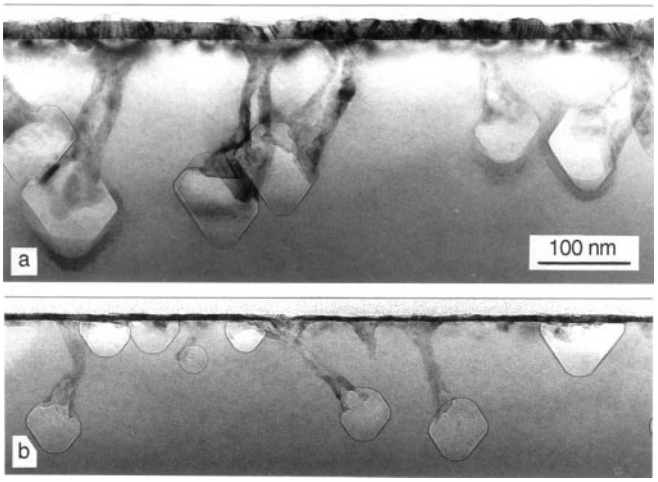

Fig. 4a,b. TEM cross-section results of the carbonization experiments #594 (**a**) and 606 (**b**). Micropipes of increasing diameters terminating in faceted bubbles within the silicon substrate. Some pyramidal voids in (**b**). Note the different defect sizes and SiC layer thicknesses

the same magnification. They show some micropipes with strongly {111} faceted bubbles at their ends inside the substrate. Also typical of these micropipes is their relatively wide crater-like opening at the interface that first decreases in diameter before increasing again towards the bubbles. On average, in sample #606 (Fig. 4b) these defect structures are smaller than in sample #594 (Fig. 4a). Voids occur in Fig. 4b only. Some much larger voids, up to 0.3 μm in edge length and already bridged by the SiC layer, occur in cross-sections of sample #594, in agreement with the SEM results mentioned above. The two images of Fig. 4 clearly reveal a distinct difference in the SiC layer thickness, which corresponds to the different volume fractions of the silicon substrate consumed during the two carbonization processes. Measurements and correlations of the SiC layer thickness are described in detail in Sect. 2.2.4, and summarized in Table 1.

A more reliable analysis of the defect structure of different samples is achieved by TEM on plan-view specimens that are chemically thinned almost to perforation. Images of thin sandwich samples of SiC on silicon yield information on the lateral distribution and density of micropipes with bubbles [16], and, to some extent, also of voids as will be described below. Figures 5a–d are cuts of plan-view images of samples #594, 604, 606 and 612, at the same magnification. They show micropipes with bubbles of different dimensions and densities. In Fig. 5a the largest structures have grown at the higher carbonization temperature in connection with the lowest total gas pressure and C_3H_8 flow. Carbonization using the same low pressure and gas flow but a lower temperature creates smaller structures of similar density (#604, Fig. 5b). Maintaining the gas flow and increasing the total pressure (#606, Fig. 5c), or increasing the gas flow at the lowest pressure (#612, Fig. 5d) renders the defect structures much smaller, and their densities noticeably higher. These effects can be explained qualitatively within a simple model of micropipe formation in which the gas pressure and the temperature enter as essential parameters [15, 16] (see Sect. 3).

In the plan-view images of Figs. 5a–c most of the bubbles appear faceted parallel to ⟨011⟩ directions, corresponding to {111} boundaries in the volume. Only the smallest bubbles are spherical. The faceted bubbles at the end of the micropipes are not easy to distinguish from the pyramidal voids because all the cavities appearing bright, including the extremely rectangular ones which should be voids, show micropipe features associated with them. This observation again proves that voids preferentially form in places where a micropipe already exists. Several large, nearly spherical or round, cavities are surely bubbles formed by the interaction of growing micropipes as described in [16]. In contrast, the large rectangular areas of Fig. 5a denoted by V are most likely voids.

The densities of micropipes determined from larger areas of images like Figs. 5a–d are between $4 \times 10^9\,\mathrm{cm}^{-2}$ and about $1.2 \times 10^{10}\,\mathrm{cm}^{-2}$ (see Table 1). Since the voids cannot easily be identified within the high density of faceted micropipe bubbles, no void densities are given in the respective column in Table 1. “Yes” means that there were clearly distinguishable voids in the TEM cross-sections of the corresponding wafers. The TEM plan-view investigations show that an increase in the micropipe density is connected with a decrease in the average micropipe diameters. The plan-view images also confirm an increase of the diameter of the micropipes towards their end in the bubbles. There are almost no micropipes without bubbles at their tips.

A predominantly epitaxial orientation of the SiC layers with respect to the substrate can be concluded from selected area diffraction patterns, shown in Fig. 6. Figure 6a refers to a specimen area of sample #604, including the SiC layer together with a thin substrate layer and, of course, SiC within the pipes. In addition to strong diffraction spots of cubic SiC well-oriented to the corresponding silicon spots, there are intensities caused by double diffraction, and also weak intensities of a certain polycrystalline SiC portion on some indicated diffraction rings. Combined plan-view and diffraction investigations of very thin SiC layers alone were possible for only a few samples. Small specimen windows were used from which Si was completely removed by chemical thinning. Figure 6b presents a diffraction pattern of the SiC layer and the connected SiC in pipes of wafer #602. After 10 s of carbonization, this wafer shows densities and sizes of out-diffusion defects and an SiC layer thickness comparable to that of wafers #600 and #606 (Fig. 5c). Without the Si background, besides the predominant SiC ⟨100⟩ spot pattern the intensities of a polycrystalline portion are more distinct. For comparison, Fig. 6c shows a diffraction pattern of the very thin SiC layer of wafer #614, i.e., the first wafer of the series without out-diffusion defects underneath. Besides the ⟨100⟩ spot pattern this pattern (Fig. 6c) does not show any intensities of polycrystalline SiC. There are only discrete SiC {111} spots aligned along ⟨022⟩ directions and clear streaks connected with the {020}-type spots caused by planar defects on {111} planes. These observations indicate that the polycrystalline SiC portion in the layers with micropipe defects is much higher than in the thin layers without such defects. All three diffraction patterns of Figs. 6a–c show a very weak angular broadening of the SiC diffraction spots, representing mutual small-angle misorientations (up to about 6°) of SiC islands or grains within the layers. This is well-known from earlier CVD growth results [22], and is also discussed in connection with the growth of SiC layers by molecular beam epitaxy [23]. The specimen areas selected for the diffraction patterns are about 1 μm in diameter.

In addition to the combined TEM bright-field and diffraction investigations, dark-field images were taken of planar samples, using {020} or {022}-type SiC diffraction spots for imaging. Such dark-field images, not displayed here, clearly show a decrease of the SiC grain size within the layers with increasing hydrocarbon concentration during their growth. Associated with the decreasing grain size is a corresponding increase in the density of interface defects before they finally disappear.

Comparing density and size of the defect structures in SEM and plan-view TEM images of one and the same experiment (cf. Figs. 3 and 5) reveals that the dark contrast features in the SEM images are not caused only by common pyramidal voids under the SiC layer but also by bubbles of larger size enclosed in the substrate.

Based on the TEM results (Figs. 4 and 5), these specific samples of our new experiments are characterized by relatively high densities of Si out-diffusion defects at the SiC/Si interface. There is a clear tendency to smaller sizes and higher densities with increasing hydrocarbon concentrations at the reacting substrate surface, caused by either a higher C_3H_8 gas flow or a higher total pressure.

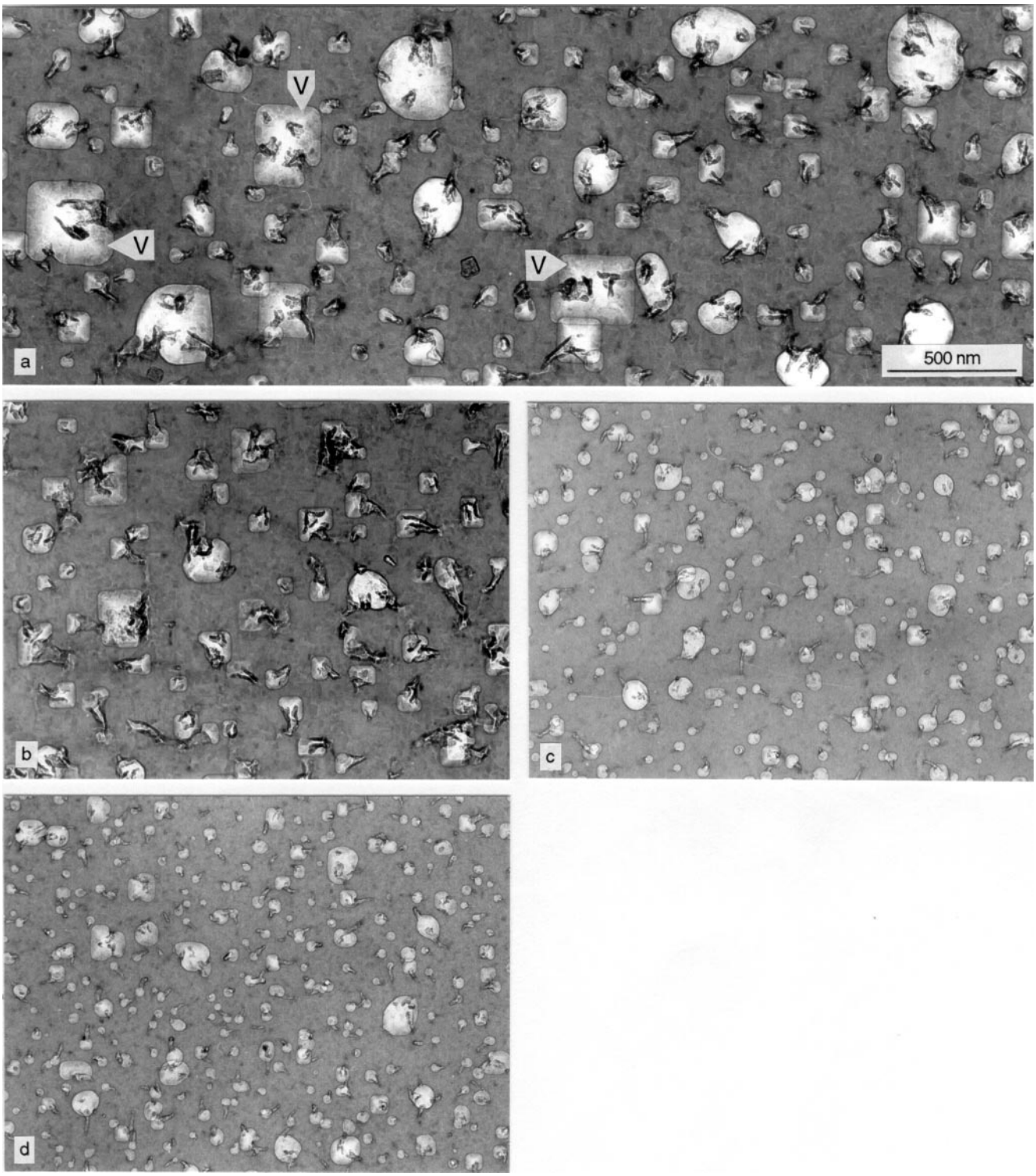

Fig. 5a–d. Plan-view TEM images (the same magnification) of thin SiC/Si sandwich samples, showing the interface defects (bubbles and voids connected with micropipes) formed under different carbonization conditions, referring to experiments #594 (**a**), 604 (**b**), 606 (**c**), 612 (**d**) (see Table 1)

2.2.3 Carbonized silicon surfaces without interface defects. For the last experiments of our series, the experimental conditions were chosen such as to completely prevent voids and micropipes, which is, of course, a prerequisite for any electronic application of these layers.

No micropipes and only a few voids were detected in the TEM cross-sections of wafers #608 and 598, at the highest total pressure for even the lowest C_3H_8 flow. Instead, there was a high density of slight depressions at the silicon surface with a thin SiC cover layer. Figure 7a represents these observations. We assume that under these carbonization conditions initial shapes of craters that have formed between the SiC islands by consuming silicon are completely covered with the growing SiC layer at quite an early stage. This does not allow

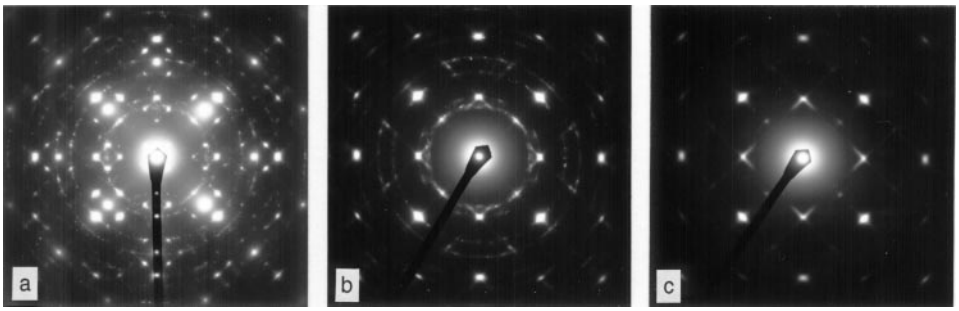

Fig. 6a–c. Selected area diffraction patterns of planar samples of wafers #604 (**a**), 602 (**b**) and 614 (**c**). Diffraction from SiC on Si in (**a**), and from SiC alone in (**b**) and (**c**)

any pipes to develop further at these sites. A further increase of the hydrocarbon fraction in experiments #616 and 626 under the same carbonization conditions also essentially suppresses the formation of the slight depressions at the substrate surface, thus reducing the interface roughness. For comparison, Fig. 7b shows a cross-section of wafer #616, which is also representative of wafer #626.

Comparing the various experiments at the lowest total pressure of 50 mbar confirms the above tendency of interface defects to disappear with increasing hydrocarbon flow. Doubling the C_3H_8 flow from 0.33 sccm for the carbonization of wafer #604, to 0.66 sccm for wafer #612, causes the smallest defects (pipes with bubbles and voids) of highest density (see Figs. 5b,d). Further increasing the hydrocarbon gas flow to 1 sccm in wafer #620, at the same low pressure, fully prevents the formation of micropipes. However, there still is a certain roughness of the SiC/Si interface due to small surface depressions, as Fig. 7c shows.

2.2.4 SiC *layers thickness as a function of the experimental parameters.* In the right-hand column, Table 1 lists the thicknesses of the SiC carbonization layers determined from TEM cross-sectional images. Medium-magnification images were used to study the thicker layers, which also showed the strongest thickness variations. In HREM images, presenting the SiC and substrate lattice structures, the SiC layers of mean thickness, and especially the very thin ones, were measured more accurately. The typical layer thickness is followed by the maximum layer thickness given in brackets. The latter refers to single tips or hills of protruding islands or grains on the surface (see, e.g., Fig. 4a) or, in some cases, (for wafers #598, 600 and 608) to sites above or around a few voids. For the thinnest SiC layers, Table 1 lists only one value or a small range of values of the layer thickness.

Figure 8 shows parts of HREM cross-section images of three different wafers of our series, with Fig. 8a referring to wafer #612, i.e., the one with the highest detected micropipe density and with an SiC layer of medium thickness. In regions between out-diffusion defects there are sections of a rather perfect SiC layer. Figure 8b shows part of the thinnest SiC layer in our series, i.e., of sample #620, with a large distribution of slight depressions on the substrate surface (see also Fig. 7c). Finally, Fig. 8c presents the somewhat thicker SiC layer grown on wafer 626, applying the highest total pressure and the highest hydrocarbon concentration. All three images of Fig. 8, the long edges of which are cut parallel to (100)-type substrate lattice fringes, reveal the stepped structure of the silicon surface corresponding to the off-axis orientation of the substrates used.

Figure 9 shows the SiC layer thickness as a function of the hydrocarbon fraction for all carbonization experiments of 60 s, at a substrate temperature of 1290 °C. In the encircled range the formation of micropipes or voids does not occur.

3 Discussion

A micropipe formation model has been discussed in detail in [15] and [16]. The description of the model includes a micropipe radius that results from two competing diffusion pro-

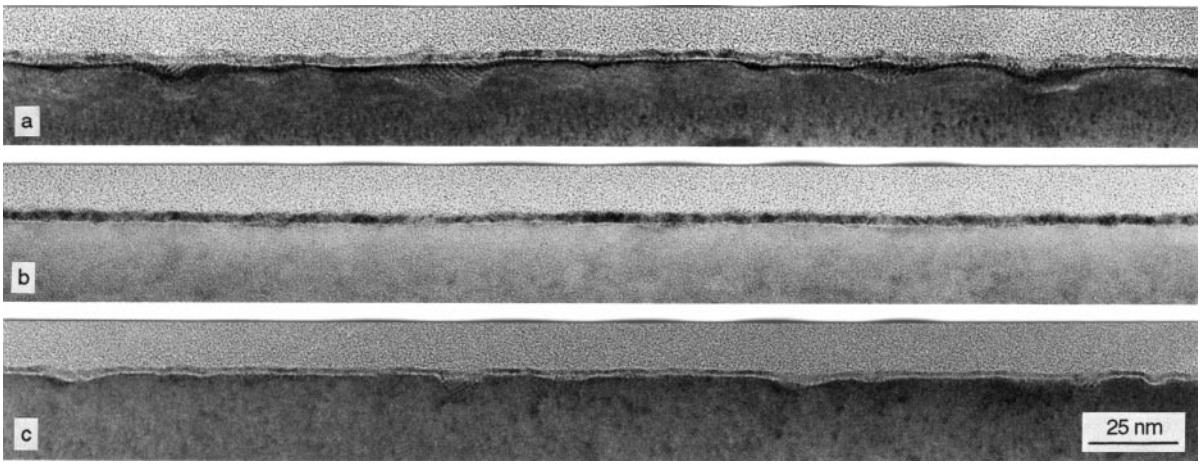

Fig. 7a–c. TEM cross-section images of experiments #608 (**a**), 616 (**b**) and 620 (**c**). Note the difference in the SiC/Si interface roughness as a function of carbonization parameters and extremely thin SiC layers

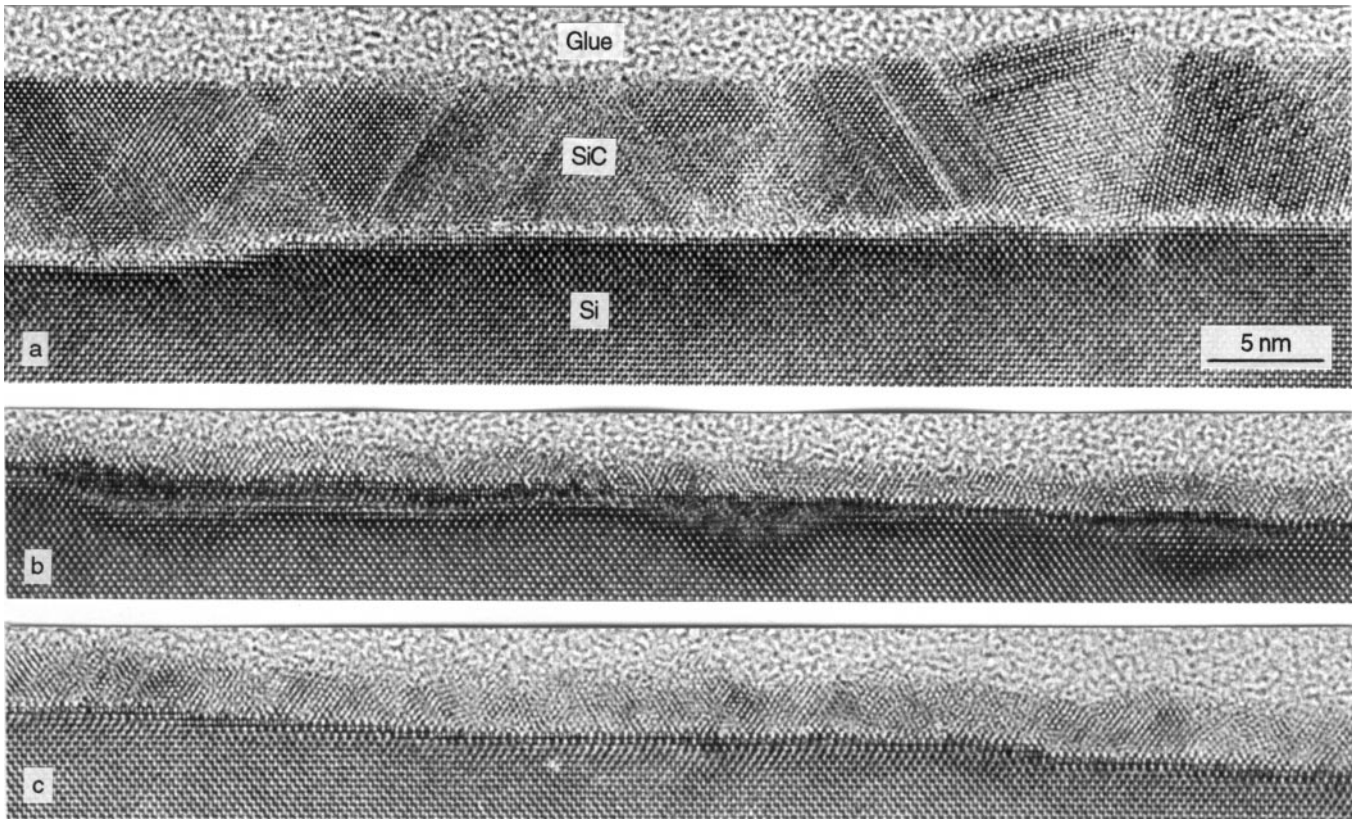

Fig. 8a–c. High resolution cross-section images of SiC layers on silicon, referring to experiments #602 (**a**), 620 (**b**) and 626 (**c**). Note the high density of planar defects in the very thin SiC layers

cesses, essentially depending on diffusivities and concentration differences of diffusing silicon and hydrocarbon species. Within this model the micropipe radius r_p is given by

$$r_p = [2D_{Si}\Delta C_{Si}t_{SiC}n_{SiC}/(D_C\Delta C_C n_{Si})]^{1/2} \quad (1)$$

where D_{Si} is the surface diffusion coefficient of silicon over a SiC covered silicon surface, D_C the gas diffusion coefficient of the hydrocarbon gas which supplies the carbon for SiC formation, ΔC_{Si} is the difference in the areal silicon concentration on the SiC layer between the bottom and the top of the micropipe, t_{SiC} the thickness of the SiC walls covering the interior of the micropipe, n_{Si} the volume density of silicon and n_{SiC} the volume density of silicon carbide. Finally, ΔC_C is the difference in the concentration of carbon in the hydrocarbon gas between the bottom and the top of the micropipe. The quantity ΔC_C is directly proportional to the corresponding difference in the pressure of hydrocarbon gas.

In our earlier experiments [16], the micropipes grew at a given constant high temperature and gas pressure and therefore the micropipe radius showed a rather narrow radius distribution. Only at the very end of the process when the micropipes were finally overgrown with SiC, the available hydrocarbon flux dropped (corresponding to a decreasing ΔC_C) with a correspondingly drastic increase in radius causing the bubble-like features at the end of many micropipes.

In the present experiments, we were able to observe the influence of changing temperature and hydrocarbon pressure. The new results obtained clearly show a decrease of the micropipe radius at the SiC/Si interface with increasing hydrocarbon concentration and/or total pressure in the CVD reactor as expected from (1). The micropipes grow during the temperature ramp and show an increasing radius towards the bubbles. Increasing temperatures lead to an exponentially increasing D_{Si} (whereas the diffusivity in the gas D_C should increase only linearly with temperature) so that, based on (1), an increasing radius with increasing temperature is expected. As pointed out earlier [15], the bubbles themselves show a drastic increase of the pipe radius by silicon out-diffusion without a remarkable further ingrowth of SiC, indicating a closure of the pipe channels by the growing SiC. The narrowest places of the pipes are assumed to be preferentially closed if the silicon out-diffusion increases with temperature, and if the effective flux of hydrocarbon gas into the pipes is reduced. The bubbles at the top of all micropipes indicate the end of pipe growth and the pipe closure due to the sealing of the substrate with SiC. Since micropipe growth does not start at the same time for all micropipes, the pipe radii differ to a certain extent within one sample. Pipes initiated at a lower temperature are expected to be smaller, to close earlier and end in smaller bubbles.

Micropipe formation under the new conditions is assumed to be possible only at sufficiently high temperatures in combination with a high density of SiC nuclei or islands, and with a certain silicon surface roughness occurring as depressions at the substrate surface. This surface roughness is now much lower than that for the SiC contamination nuclei in the former experiments. The relatively small size of the grains within the SiC layers of dark-field images corresponds to a high nucleation density. High nucleation densities are generated during

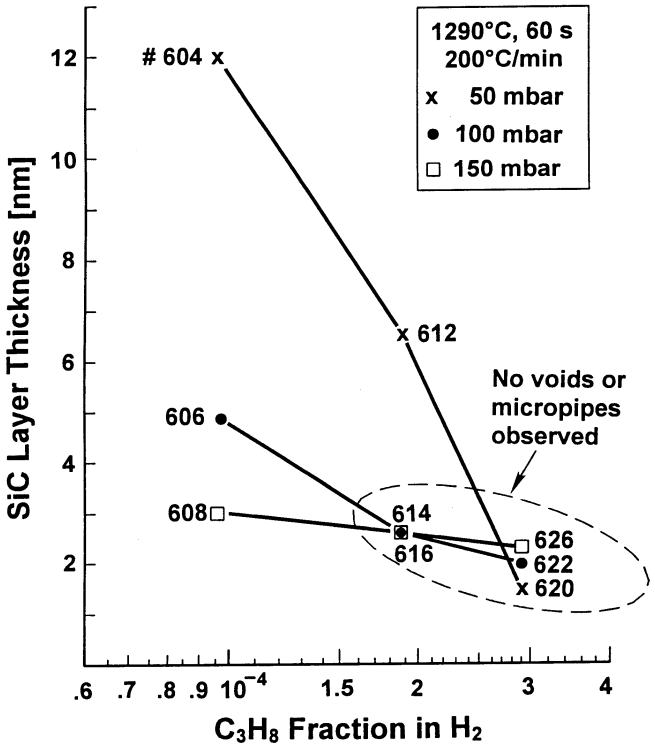

Fig. 9. SiC film thickness as a function of the C_3H_8 fraction in hydrogen for the carbonizations of 60 s at 1290 °C

the slow temperature ramp-up procedure, implying predominantly two-dimensional growth, which is in contrast to our former carbonization experiments carried out at high temperatures only. In our new series of experiments, an increase in the hydrocarbon concentration or pressure is connected with an increase in the nucleation density, and a clear decrease in the grain size, resulting in thinner and smoother SiC films. The decreasing grain size within the SiC layers is connected with a distinct increase in the density of planar defects on SiC {111} planes. The frequent occurrence of such planar defects close to the interface is most pronounced in Fig. 8c. The increase in the density of planar defects with increasing nucleation density may be understood in the framework of a proposed model of stacking fault and twin formation during heteroepitaxial growth [24]. Within this model the density of planar defects is assumed to increase in proportion to the density of SiC nuclei.

4 Conclusions

Carbonization conditions were found for the prevention of micropipes and voids at SiC/Si interfaces. The microstructures forming at the interfaces by varying the experimental conditions were investigated in detail by SEM and TEM. The appearance and the area densities of silicon out-diffusion defects depend on the total propane concentration and/or the total pressure in the CVD reactor. Associated with slow temperature ramping, these defects occur even at very low partial pressures of propane. At sufficiently high propane partial pressures, the high density of SiC nuclei prevents the formation of micropipes and voids by silicon out-diffusion. Thus, we have shown that it is possible to attain microscopically sharp defect-free SiC/Si interfaces under optimized carbonization conditions, even in CVD processes, which are performed at much lower pressures than previously used for the prevention of interface defects such as voids [13]. The reason why already lower hydrocarbon pressures are sufficient to prevent the formation of out-diffusion defects appears to be associated with the slow temperature ramp-up we used which allows the development of a sufficiently high density of SiC nuclei. Finally, we mention specifically that in the cases in which out-diffusion defects such as micropipes and voids are prevented, the density of {111} stacking faults and twins in the SiC layer becomes particularly high.

Acknowledgements. The authors would like to thank Mrs S. Hopfe and B. Lausch for preparing numerous TEM specimens, and Mrs U. Doss for her assistance at the SEM.

References

1. R.F. Davis, G. Kelner, M. Shur, J.W. Palmour, A.J. Edmond: Proc. IEEE **79**, 677 (1991)
2. *Properties of Silicon Carbide*, ed. G.L. Harris (INSPEC, London 1995)
3. S. Nakamura, G. Fasol: *The Blue Laser Diode* (Springer, Berlin 1997)
4. L. Di Cioccio, Y. Le Tiec, F. Letertre, C. Jaussaud, M. Bruel: Electron. Lett. **32**, 1144 (1996)
5. Q.Y. Tong, T.H. Lee, P. Werner, U. Gösele, R.B. Bergmann, J.H. Werner: J. Electrochem. Soc. **144**, L111 (1997)
6. S. Nishino, J.A. Powell, H.A. Will: Appl. Phys. Lett. **42**, 460 (1983)
7. A. Addamiano, J.A. Sprague: Appl. Phys. Lett. **44**, 525 (1984)
8. J.A. Powell, L.A. Matus, M.A. Kuczmarski: J. Electrochem. Soc. **134**, 1558 (1987)
9. H.J. Kim, R.F. Davis, X.B. Cox, R.W. Linton: J. Electrochem. Soc. **134**, 2269 (1987)
10. B. Molnar, L.M. Shirey: Mater Res. Soc. Symp. Proc. Vol. **162**, 457 (1990)
11. A.J. Steckl, J.P. Li: IEEE Trans. Electron Devices **39**, 64 (1992)
12. C.C. Chiu, S.B. Desu: J. Mater. Res. **8**, 535 (1993)
13. J.P. Li, A.J. Steckl: J. Electrochem. Soc. **142**, 634 (1995)
14. G. Ferro, Y. Monteil, H. Vincent, V. Thevenot, M.D. Tran, F. Cauwet, J. Bouix: J. Appl. Phys. **80**, 4691 (1996)
15. R. Scholz, U. Gösele, E. Niemann, D. Leidich: Appl. Phys. Lett. **67**, 1453 (1995)
16. R. Scholz, U. Gösele, E. Niemann, F. Wischmeyer: Appl. Phys. A **64**, 115 (1997)
17. R. Scholz, U. Gösele, E. Niemann, D. Leidich, F. Wischmeyer: Submitted to Conf. Proc. of the *1st European Conference on Silicon Carbide and Related Materials*, Heraklion, Crete, Greece, October 6–9, 1996, to be published in Diamond Relat. Mater.
18. A.J. Fleischman, C.A. Zorman, M. Mehregany, C. Jacob, S. Nishino, P. Pirouz: In *Proc. Sixth Int. Conf. on Silicon Carbide and Related Materials*, (Kyoto, Sept. 18–21, 1995), ed. by S. Nakashima, H. Matsunami, S. Yoshida, H. Harima, Inst. of Phys. Conf. Ser. No. 142 (Inst. of Phys. Publ., Bristol 1996) pp.197–200
19. I. Kusunoki, M. Hiroi, T. Sato, Y. Igari, S. Tomoda: Appl. Surf. Sci. **45**, 171 (1990)
20. A.J. Steckl, J.P. Li: Mater. Res. Soc. Symp. Proc. Vol. **242**, 537 (1992)
21. K. Zekentes, N. Becourt, M. Androulidaki, K. Tsagaraki, J. Stoemenos, J.M. Bluet, J. Camassel, J. Pascual: Appl. Surf. Sci. **102**, 22 (1996)
22. M. Iwami, M. Hirai, M. Kusaka, Y. Yokota, H. Matsunami: Jpn. J. Appl. Phys. **28**, L293 (1989)
23. K. Zekentes, V. Papaioannou, B. Pecz, J. Stoemenos: J. Cryst. Growth **157**, 392 (1995)
24. P. Pirouz: In *Polycrystalline Semiconductors*, Springer Proc. in Physics, Vol. 35, ed. by J.H. Werner, H.J. Möller, H.P. Strunk (Springer, Berlin 1989) pp. 200–212